EUROPEAN COMMISSION

Community research

GOBIERNO DE ESPAÑA | MINISTERIO DE ECONOMÍA Y COMPETITIVIDAD | Ciemat Centro de Investigaciones Energéticas, Medioambientales y Tecnológicas

Long-term Performance of Engineered Barrier Systems

PEBS

Long-term Performance of Engineered Barrier Systems PEBS

Long-term THM tests reports: THM cells for the HE-E test: update of results until February 2014

(DELIVERABLE-N°: D2.2-7.3)

Contract (grant agreement) number: FP7 249681

CIEMAT Technical Report CIEMAT/DMA/2G210/03/2014

Author(s):

M.V. Villar, P.L. Martín, F.J. Romero

Reporting period:

Date of issue of this report: March 7th 2014

Start date of project: 01/03/10 Duration : 48 Months

Project co-funded by the European Commission under the Seventh Euratom Framework Programme for Nuclear Research &Training Activities (2007-2011)		
Dissemination Level		
PU	Public	**PU**
RE	Restricted to a group specified by the partners of the [acronym] project	
CO	Confidential, only for partners of the [acronym] project	

EURATOM

Contents

Acknowledgements

The research leading to these results has received funding from the European Atomic Energy Community's Seventh Framework Programme (FP7/2007-2011) under Grant Agreement n°249681, the PEBS project. This work is being additionally financed by ENRESA through a CIEMAT-ENRESA General Agreement.

1 Introduction

A common design of a high-level radioactive waste (HLW) disposal system consists of the wastes encapsulated within steel canisters that are emplaced within horizontal tunnels, with the space between the canisters and the surrounding rock filled with a bentonite-based material. In the early post closure period the buffer is expected to experience the maximum temperature. In this phase the buffer is largely unsaturated and the thermal evolution of the EBS is likely to be controlled by the effective thermal conductivity of dry buffer.

In particular, the temperature evolution of the engineered barrier system and surrounding rock was simulated using reference data for the thermal properties of HLW, bentonite backfill and Opalinus Clay. The results showed that the surface temperatures would reach a maximum value of ~150°C within a few years after emplacement (Johnson *et al*. 2002). These anticipated temperatures at the canister surface, in the bentonite and at the bentonite-host rock interface were scaled down in time and space to meet the specifications of the HE-E experiment, which is being carried out in the framework of PEBS (Gaus *et al*. 2011). The HE-E experiment targets the period immediately after repository closure when the temperatures are maximal and the moisture content is low but increasing.

The HE-E experiment is a 1:2 scale heating experiment considering natural resaturation of the EBS and a maximum heater surface temperature of 140°C. Heater temperature increased almost linearly to its maximum value in a period of one year after which the temperature was held constant. The experiment is located at the Mont Terri URL (Switzerland) in a 50-m long non-lined horizontal microtunnel of 1.3 m diameter excavated in 1999 in the shaly facies of the Opalinus Clay. The test section of the microtunnel was characterised in detail during the Ventilation Experiment (ENRESA 2005). The detailed design of the experiment is described in Teodori & Gaus (2011).

The experiment consists of two independently heated sections (Figure 1), where the heaters are placed in a steel liner supported by MX80 bentonite blocks (dry density 1.81 g/cm^3, water content 10.3%). The two sections are fully symmetric apart from the granular material filling the rest of the gallery: whereas section 1 is filled with pure MX80 bentonite pellets, section 2 is filled with a 65/35 granular sand/bentonite mixture with the characteristics described below:

- Granular bentonite (B) is used in one section of the test, corresponding to the Swiss disposal concept. It is the same as the one used for the ESDRED project, mixture type E (sodium bentonite MX-80 from Wyoming). The material is described in detail in Plötze & Weber (2007). Once emplaced its water content was 5.9% and the dry average density was 1.46 kg/m^3.
- Sand/bentonite (S/B) mixture (having a higher thermal conductivity) is used in the other section. The sand/bentonite mixture was provided by MPC (Limay, France). The components are 65 % of quartz sand with a grain spectrum of 0.5 – 1.8 mm and 35 % of sodium bentonite GELCLAY WH2 (granular material of the same composition as MX-80) of the same grain spectrum, which was obtained by crushing and sieving from the qualified raw material. Water content was 13% for the bentonite and 0.05% for the sand, giving a total water content of the mixture in the range of 4%. There is some uncertainty about the actual emplaced density of the mixture, and values as low as 1.26 g/cm^3 have been given. However, based on the tests performed to check the emplacement technique, a value of 1.5 g/cm^3 has been taken for the calculations and the laboratory tests.

A heater system, capable of representing the temperature curve of the anticipated heat production in the canisters (up to a maximum of 140°C), was switched on the 28th June 2011. During the experiment the temperature, humidity and the water saturation are monitored through a system of sensors on the heater surface within the liner, in the bentonite and in the surrounding host rock.

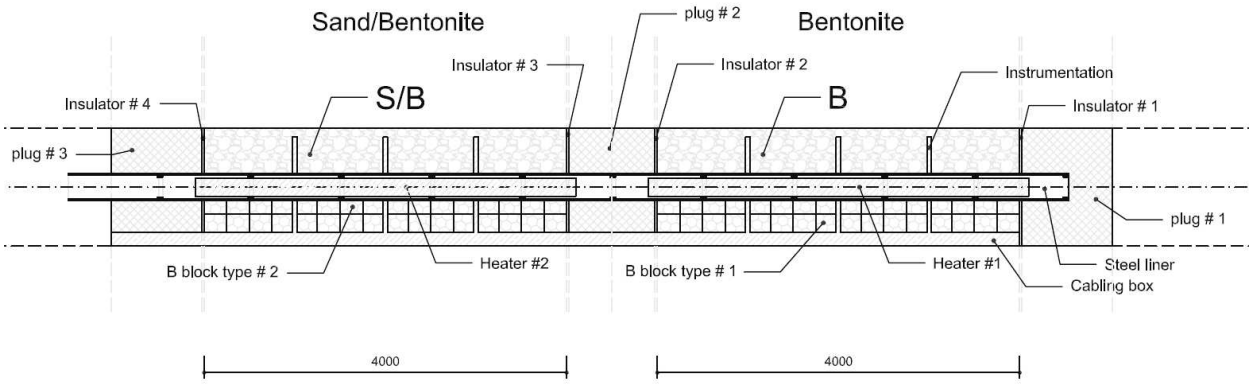

Figure 1: Layout of the *in situ* HE-E experiment

The performance of tests at different scales, in both the laboratory and the field, is very useful to observe the thermo-hydro-mechanical processes taking place in the engineered barriers and the geological medium. They also provide the information required for the verification and validation of mathematical models of the coupled processes and their numerical implementation. The laboratory tests in cells are particularly helpful to identify and quantify processes in a shorter period of time and with less uncertainty regarding the boundary conditions than the *in situ* tests. In the tests in cells the sealing material is subjected simultaneously to heating and hydration in opposite directions, in order to simulate the conditions of the clay barrier in the repository, i.e. the interaction of the water coming from the host rock and the thermal gradient generated by the heat emitted by the wastes in the canisters. With the aim of complementing the information provided by the HE-E *in situ* test, CIEMAT undertook, in the framework of the PEBS project, the performance of two tests in cells simulating the conditions of the sealing materials used in the two sections of the *in situ* test. The results obtained until the end of the PEBS project (February 2014) are given in this report, which is a continuation of Deliverable 2.2-7.1 (Villar et al. 2012). The details given in the latter are not given again in this report, but just summarised.

2 Material

The materials used in the cells are the same as those used in the *in situ* test and were sent to CIEMAT directly from the Mont Terri test site. A plastic bucket with 25 kg of the sand/bentonite mixture (S/B) was received at CIEMAT on April 2011 and 20 kg of the bentonite pellets (B) were received on June 2011 (Figure 2). The as-received water content of the materials was 6.4% for the pellets and 3.6% for the sand/bentonite mixture. The granulometric curve of both materials obtained by dry sieving is shown in Figure 3. It was checked that the granulometric curve of the bentonite granulate received at CIEMAT coincide with the granulometric curves of the material used for the ESDRED experiment (Villar et al. 2012).

Figure 2: Appearance of the materials received at CIEMAT: MX-80 pellets (left) and sand/bentonite mixture (right)

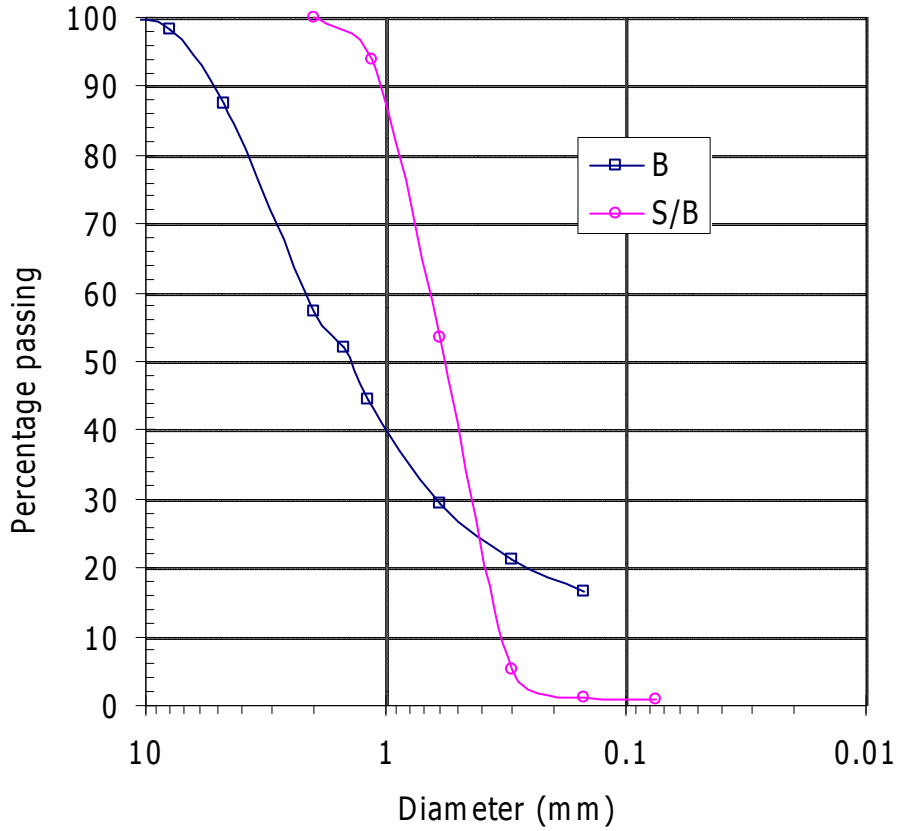

Figure 3: Granulometric curve obtained by dry sieving of the two materials used in the tests (B: bentonite pellets, S/B: sand/bentonite mixture)

The dry density of the solid grains determined with pycnometers using water as dispersing agent was 2.71 g/cm^3 for the mixture and 2.75 g/cm^3 for the granulate. The external specific surface area determined by the 9-point BET method was 5 m^2/g for the mixture and 33 m^2/g for the pellets. The superficial thermal conductivity of both materials in their as-received state was determined at room temperature using the transient hot wire method. Values of 0.33 and 0.12 W/m·K were obtained for the mixture and the granulate, respectively. The specific heat capacity of both materials ground and dried at 110°C was determined in a TG-DSC Setsys Evolution 16 equipment. The determinations were performed in the range of temperatures

from 22 to 298°C. The values obtained for the mixture ranged between 0.74 J/g·K (at 22°C) and 0.90 J/g·K (at 115°C), and for the pellets between 0.64 J/g·K (at 22°C) and 0.97 J/g·K (at 115°C) (Fernández 2011). The pore size distribution of the uncompacted materials was obtained by mercury intrusion porosimetry. The S/B mixture has a predominant macroporosity with a pore mode about 204 µm, whereas in the B pellets mesopores of pore mode about 0.014 µm predominate (Villar 2013).

The swelling pressure of small samples (3.8 or 5.0 cm in diameter, 1.2 cm in height) of MX-80 bentonite powder compacted with its hygroscopic water content at dry densities between 1.1 and 1.8 g/cm^3, was determined at CIEMAT at room temperature using deionised water as saturation fluid. The swelling pressure (P_s, MPa) could be related to final dry density (ρ_d, g/cm^3) through the following empirical expression (Villar 2013):

$$\ln P_s = 5.44\ \rho_d - 6.94 \qquad [1]$$

According to this fitting, for a dry density of 1.53 g/cm^3 a swelling pressure of about 4 MPa is expected. The swelling pressure of the sand/bentonite mixture was determined in the same standard oedometers in samples initially compacted at a nominal dry density of 1.45 g/cm^3. An average swelling pressure of 1.5 MPa was obtained for the samples saturated with deionised water and of 0.7 MPa for the samples saturated with Pearson water, which is a sodium-chloride water with a salinity of 19 g/L reproducing the host rock pore water (Pearson 1998). Its chemical composition is indicated in Table I.

Table I: Chemical composition of the water used in the tests (mg/L)

Cl^-	SO_4^{2-}	HCO_3^-	Mg^{2+}	Ca^{2+}	Na^+	K^+	Sr^+	pH
10636	1354	26	413	1034	5550	63	47	7.6

3 Experimental setup

In the tests in cells a column of material is hydrated through the upper surface whereas the lower surface is heated at a constant temperature. The infiltration tests for the HE-E are being performed in cylindrical cells similar to the cells already used during the FEBEX and NF-PRO projects (Villar *et al*. 2005a, b, 2008). The nominal internal diameter of each cell is 7 cm and inner length 50 cm, therefore, those are the dimensions of the sample columns. The bodies of the cells were made of Teflon PTFE (thermal conductivity 0.25 W/m·K) to prevent as much as possible lateral heat conduction. The cell with bentonite pellets (called hereafter B) was externally covered with steel semi-cylindrical pieces to avoid the deformation of the Teflon caused by the bentonite swelling. This cover was not necessary in the bentonite/sand mixture cell (call hereafter S/B). Finally, the body of the cells was wrapped with insulation wool to avoid the heat loss (Figure 4).

The bottom part of the cells has a plane stainless steel heater, and the power supplied to the resistance is measured online. Inside the upper steel plug of the cells there is a deposit in which water circulates at room temperature. In this way, a constant temperature gradient between top and bottom of the sample is imposed. Hydration takes place through the upper lid of the cell. Pearson water is supplied from a deposit hanging from an electronic load cell, and the water intake is measured by changes in the weight of the deposits. Since the water availability

at the Mont Terri gallery is very limited, only a small pressure, given by an equivalent 60-cm high water column, was applied to the saturation water.

Between the hydration piece and the upper plate, a ring load cell was located in cell B with the aim of measuring the axial pressure during the test. The walls of the cells were perforated for the installation of capacitive-type sensors placed in the middle of the columns at three different levels (10, 22 and 40 cm from the heater approximately). The transducers used are VAISALA HMT334 protected by cylindrical stainless steel filters. The accuracy of the humidity sensor is ±1% over the range 0-90 percent RH and ±2% over the range 90-100 percent RH.

The water volume intake, the heater power, the axial pressure (in cell B), and the relative humidity (RH) and temperature (*T*) at different levels inside the clay are being measured as a function of time. A schematic diagram of the setup is shown in Figure 5. The different components of the system were described in detail in Villar et al. (2012).

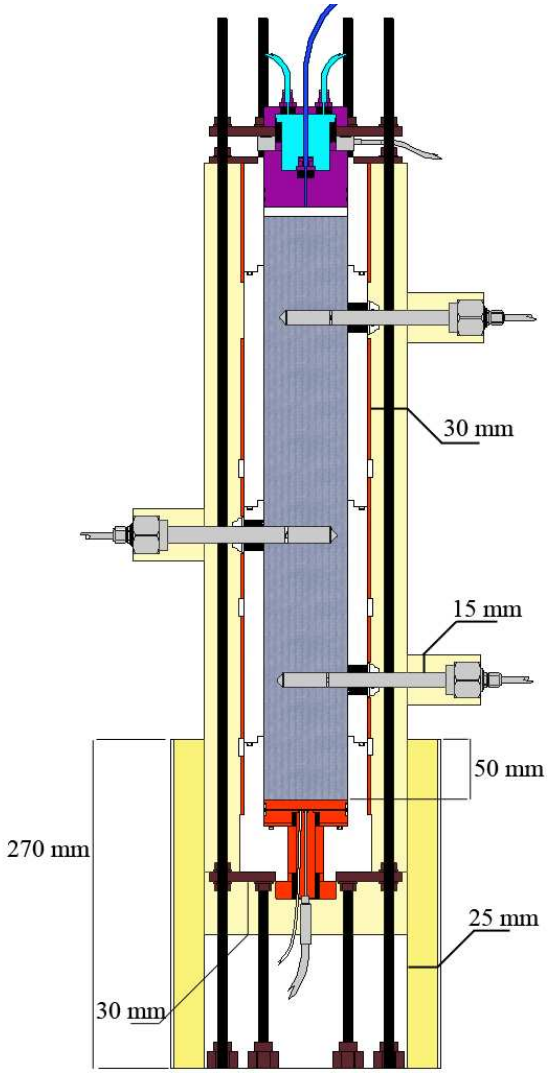

Figure 4: Cell B with the external isolation

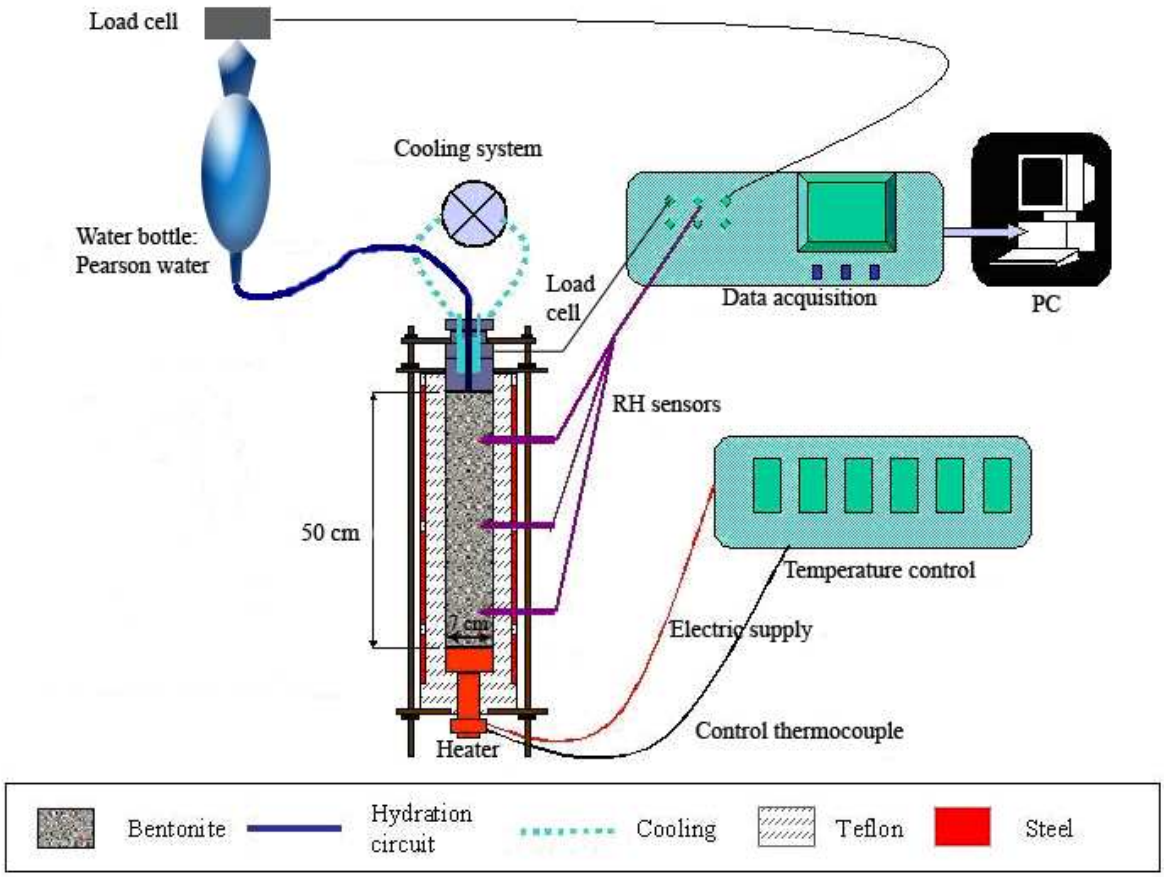

Figure 5: Experimental setup for the infiltration tests

4 Methodology

4.1 FABRICATION OF THE COLUMNS

The columns were manufactured by filling the cells in seven 7-cm high layers. The material was just poured inside the cell. The quantity of material was computed taking into account the initial water content, the inner volume of the cells (7 cm in diameter and a target height of 50 cm) and the nominal dry density, which was 1.45 in the case of cell S/B and 1.47 in the case of cell B. To fill the pellets cell a funnel was used to avoid the loss of the finer particles. No compaction energy was needed to manufacture the bentonite pellets column, whereas a very low energy was applied to the mixture: 5 to 10 strokes with a 2.5-kg Proctor rammer with a 30.5 cm drop to each of the 7 layers.

Between the clay and the upper closing, a 70-mm diameter and 8-mm high porous stone was placed. The top plug with the o-rings around was pushed to its place and tightened. This assembly was weighed and afterwards, the perforations for the insertion of the sensors were drilled in the bentonite through the Teflon walls. The assembly was weighed again in order to know how much material had been lost as a consequence of drilling. Thus the initial characteristics of the columns were obtained (Table II). The differences with respect to the target values are due to the compression of the column caused by the upper plug tightening. Figure 6 (right) shows the aspect of the cells in its final configuration.

Table II: Characteristics of the samples after compaction

	S/B	B
Initial water content (%)	3.6	6.4
Sample mass (g)	2949	3094
Sample mass after drilling (g)	2930	3076
Volume of sensors (cm^3)	18	20
Theoretical dry mass (g)	2828	2891
Diameter (mm)	70.7	70.0
Height (mm)	494.6	483.9
Dry density (g/cm^3)	1.45	1.53
Porosity	0.463	0.444
Void ratio	0.863	0.797
Degree of saturation (%)	11	22

Figure 6: Cell B before being wrapped with the insulation material (left) and THM cells in operation (right)

4.2 TESTS INITIATION

Once the cell was mounted and the sensors inserted, the data acquisition was launched. A brief period to check the initial stabilisation and the correct working of the sensors was taken. This period lasted 140 hours for cell B and 260 h for cell S/B. The temperatures recorded by the three sensors in each cell were nearly identical and reflected the laboratory changes. For the relative humidity the differences inside the same column were below 1%, with average values of 40% in cell B and 46% in cell S/B.

Accidentally, the valve giving access to hydration was opened in cell S/B for a few minutes (about 5 min), and due to the high permeability of the material, this caused the relative humidity in the upper part of the column to increase. The average water content of the column increased from 3.6 to 4.7%.

5 Results

5.1 CELL S/B

5.1.1 Initial heating

In the case of the test performed with the sand/bentonite mixture (cell S/B), 260 h after starting data acquisition the heater temperature was set at 100°C and the cooling system on top kicked off, and this time is considered as t=0 for the rest of the test. The target temperature was reached in 25 min, but the stabilisation of the temperature registered by the sensors took approximately 30 h, and much longer for the relative humidity. After 7 h of heating the cell was wrapped with an isolating material and this was clearly reflected in an increase of the temperature inside the mixture and affected as well the relative humidity. After 1566 h the isolation material was changed, and again modified after 1666 h, what improved the longitudinal heat transmission inside the column and increased the temperature inside the mixture. The two sensors farther from the heater reflected an increase in relative humidity from the beginning of heating, more intense for the middle sensor from the moment the temperatures near the heater increased. Both sensors recorded a stable and similar RH value approximately after 2200 h. However, the sensor placed at 10 cm from the heater recorded a sharp initial increase up to a value of RH 70%, but after 120 h it started to decrease, more intensely when the isolation was improved. A quasi-stable value of 36% was reached after 2400 h. This evolution of the relative humidity along the column reflected the migration of water in the vapour phase from the material close to the heater towards cooler zones. Once the relative humidity inside the column stabilised, the heater temperature was increased to 140°C, final target temperature, in 12 min. The temperatures inside the mixture stabilised after 24 h, and the relative humidity in approximately 1130 h.

The equilibrium values of T and RH at the end of the heating phases with heater temperature at 100°C and 140°C are shown in Figure 7.

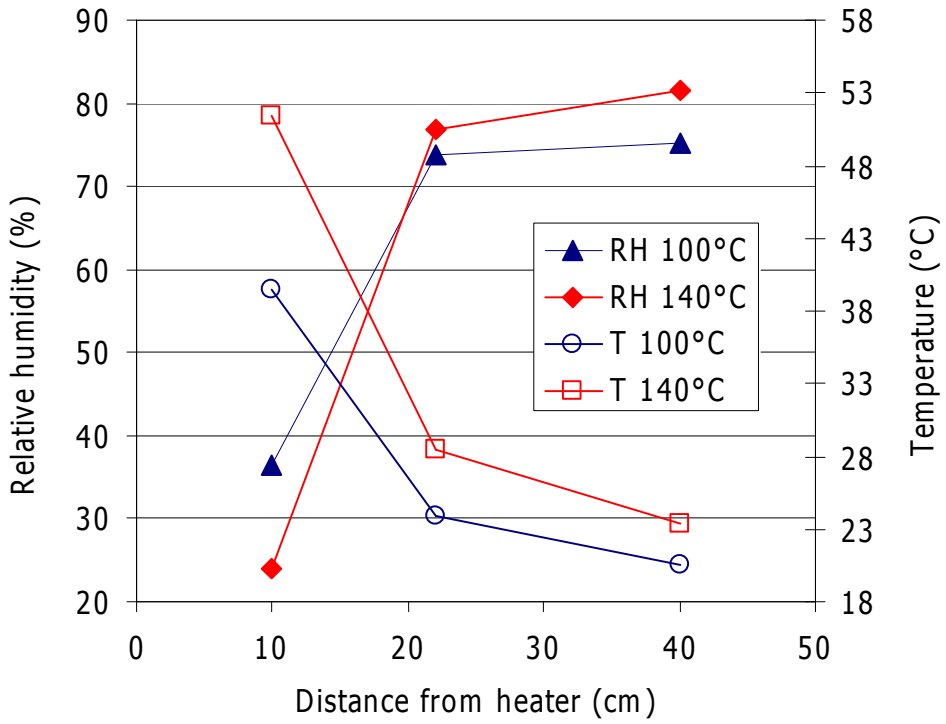

Figure 7: Equilibrium values measured inside the material when the heater was set to 100°C (*t*=2400 h) and 140°C (*t*=3620 h) in cell S/B

5.1.2 Heating and hydration

After the stabilisation of RH and *T* for a heater temperature of 140°C, the hydration line was opened. Only a small pressure, equivalent to a 60-cm high water column, was applied to the saturation water.

Figure 8 shows the evolution of *T* and RH recorded by the sensors after the beginning of hydration. The temperatures kept the same as before hydration for some days. As the water front approached the sensors, the temperatures started to increase, so the simultaneous increase in temperature and relative humidity took place first in sensor 1 (after approx. 44 h), then in sensor 2 (after approx. 160 h) and finally in sensor 3 (after approx. 235 h). The coupling between the increase in water content and that of temperature can be clearly seen in the Figure. For sensor 3, placed in the hottest area, the arrival of the water front caused a temporary decrease in temperature that was quickly recovered. The overall increase in temperature due to the increase in water content was of 6°C for sensor 1, 14°C for sensor 2 and 16°C for sensor 3.

Figure 9 shows the evolution of temperature and relative humidity inside the column and the water intake until the end of February 2014. The temperatures inside the material kept steady, oscillating according to the laboratory temperatures, particularly in the upper part of the column. Thus, for sensor 1 the average steady temperature was 27±2°C, for sensor 2 was 40±1°C and for sensor 3 was 64±1°C. With respect to the RH evolution, its increase was very sudden once the water front reached the area where the sensors are placed. Consequently the sensors became quickly flooded and started recording faulty values (except for sensor 1 which recorded a RH value of 98%). Sensor 1 started recording 98% approximately 135 h after hydration started, sensor 2 after 235 h and sensor 3 after 387 h. The overall water intake was also very large until the bottom sensor became flooded, and then the water intake rate softened (continuous line in Figure 9, right). In fact, air bubbles could be seen in the hydration

line, and these were periodically purged, since they seemed to hinder the water inflow. This is the reason why the water intake curve is not smooth, because after purging, the water intake was temporarily accelerated. According to the water intake measurements, after 16370 h of hydration (682 days) the overall water content of the mixture was 33% and its degree of saturation 104%.

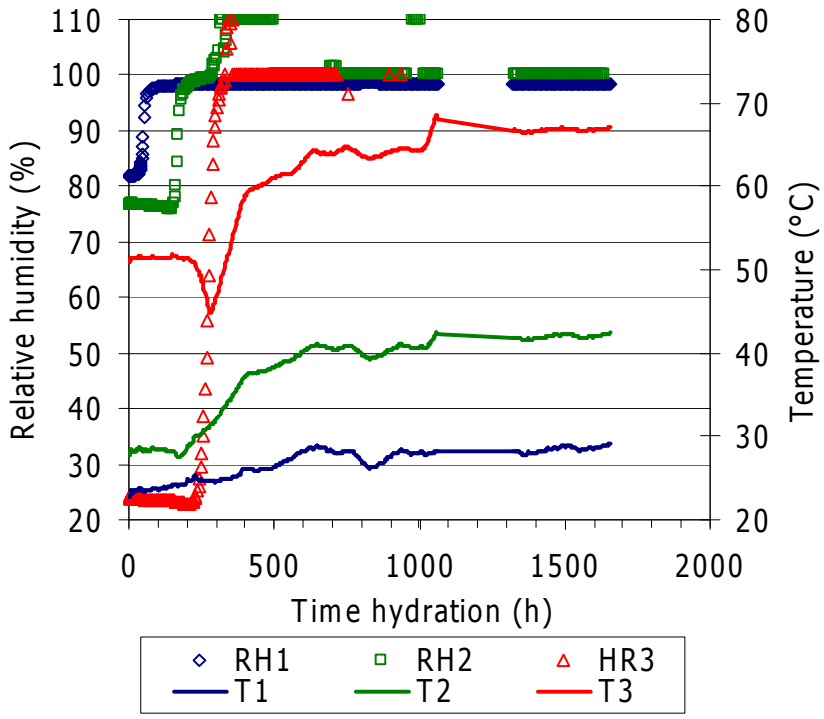

Figure 8: Evolution of *T* and RH in cell S/B after the beginning of hydration (sensor 1 placed at 40 cm from the bottom, sensor 2 at 22 cm and sensor 3 at 10 cm)

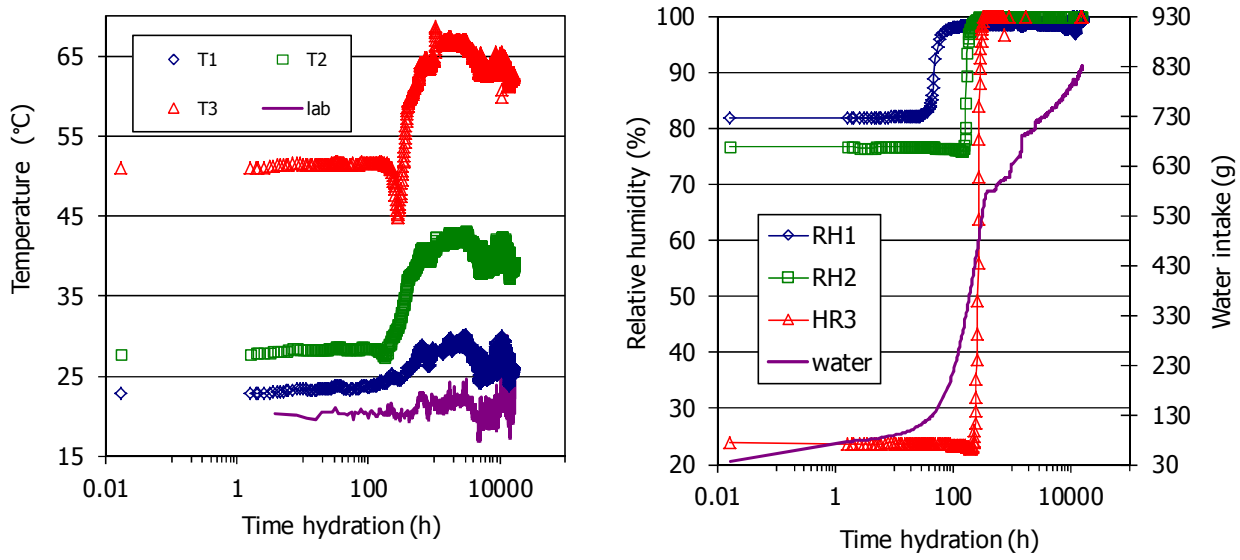

Figure 9: Evolution of *T* (left) and RH (right) in cell S/B after the beginning of hydration (sensor 1 placed at 40 cm from the bottom, sensor 2 at 22 cm and sensor 3 at 10 cm)

The temperatures on the surface of the cell were measured periodically in the last months with thermocouples placed on the surface of the cell, i.e. on the Teflon, at the same levels as the sensors inserted in the column but on the opposite side of the column (Figure 10). The

temperatures at the same level on the surface of the isolating material were also measured (Figure 11). Figure 12 shows the average of these temperatures from June 2013 (when the first external measurements were taken) to February 2014 at the different positions measured.

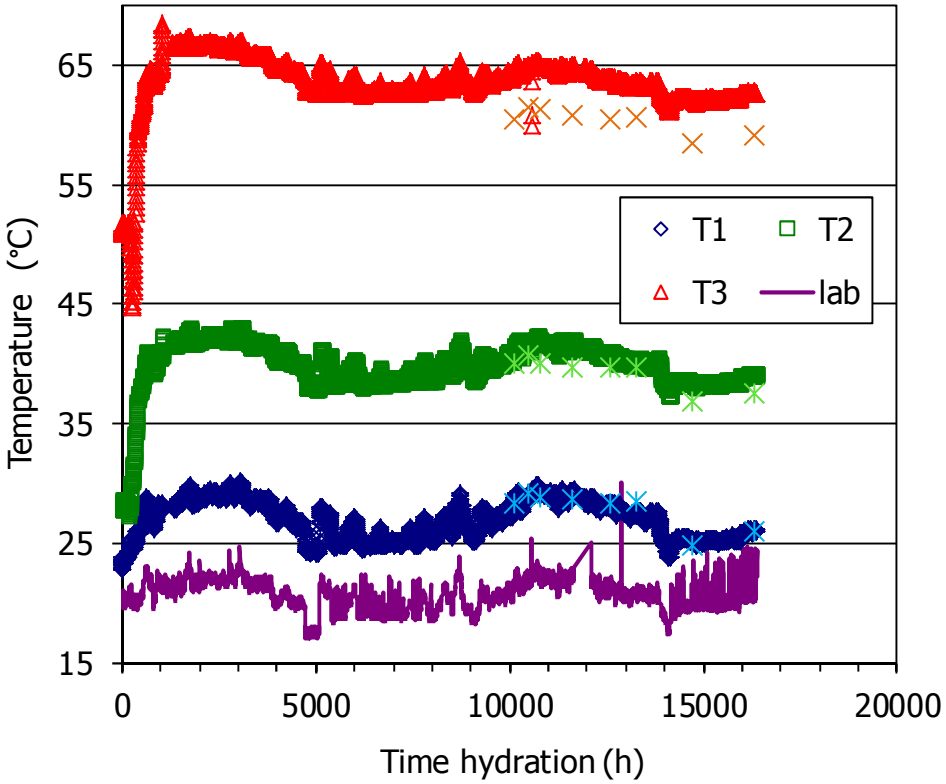

Figure 10: Evolution of temperature inside the column and on the Teflon surface (crosses) during the hydration phase (T1 at 40 cm from the bottom, T2 at 22 cm and T3 at 10 cm)

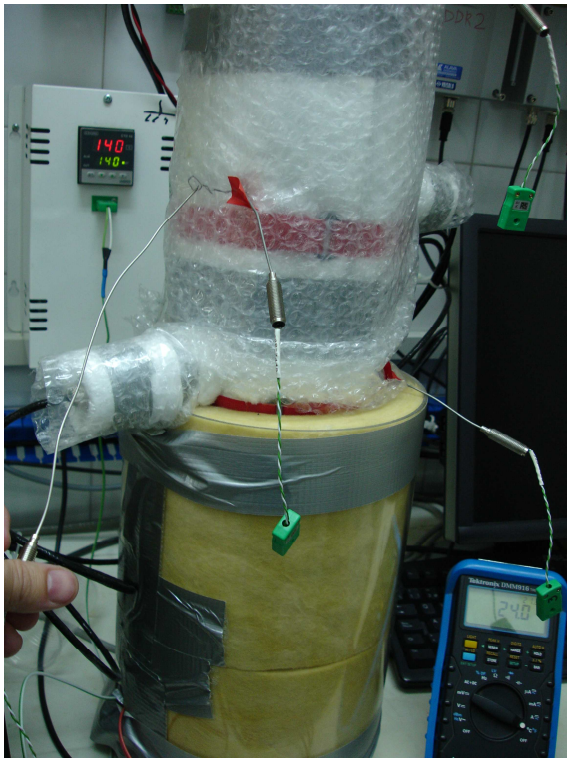

Figure 11: Measurement of temperature with thermocouples on the cell surface and on the surface of the isolating material

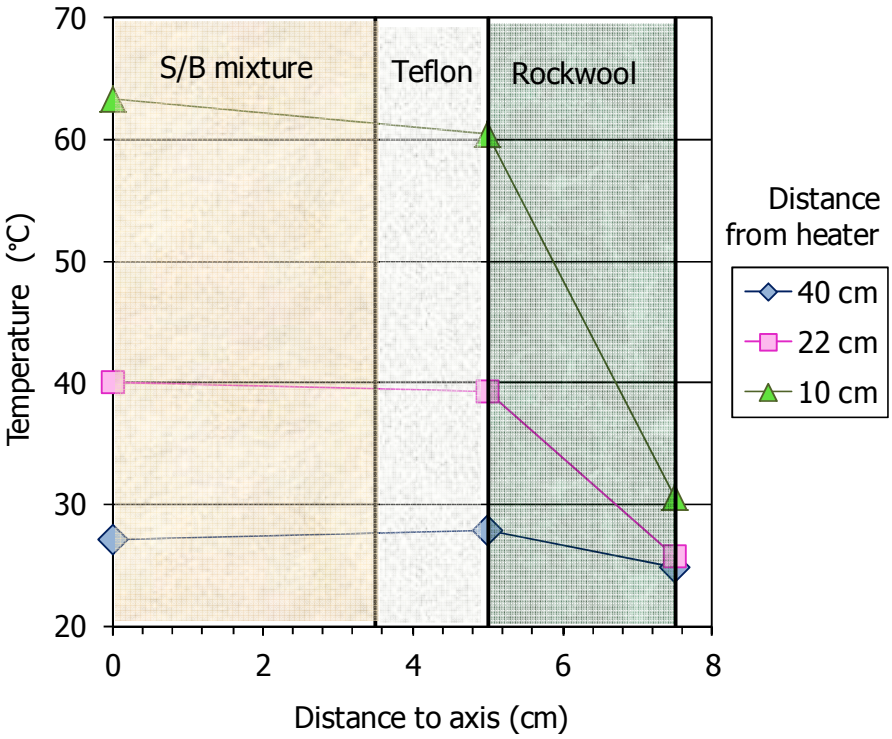

Figure 12: Average temperatures at different distances from the heater in cell S/B from June 2013 to February 2014 (average laboratory temperature in this period 20.9±1.2°C)

The heater power was also measured during all the test phases. The improvement of the isolation induced a decrease of the heater power from 10.7 to 6.6 W to keep the target temperature of 100°C at the heater surface. When the heater temperature was increased to 140°C, the heater power increased to 10 W. Upon hydration, the arrival of water to the heater area gave place to a progressive increase of heater power up to a value of 12 W, which has remained approximately constant (12.2±0.4 W) so far (Figure 13).

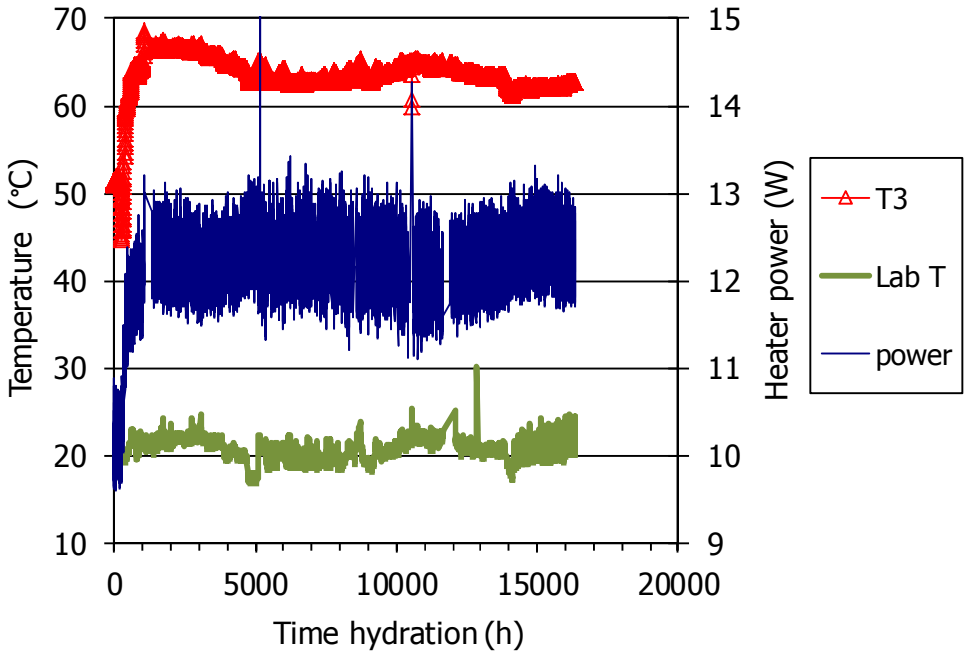

Figure 13: Laboratory temperature, heater power and temperature at 10 cm from the heater (sensor 3) in cell S/B during the hydration phase of the test

A summary of the values recorded during the whole hydration phase is given in Table A- I in Appendix 1.

5.2 CELL B

5.2.1 Initial heating

In the test performed with the bentonite pellets (cell B), 160 h after starting data acquisition the heater temperature was set at 100°C and the cooling system was kicked off, and this time is considered as *t*=0 for the rest of the test. The target temperature was reached in 33 min, but the stabilisation of the temperature registered by the sensors took approximately 20 h, and much longer for the relative humidity.

The isolation was reinforced 1500 hours after heating started, and the temperature inside the bentonite increased. Once the relative humidity inside the column stabilised, the heater temperature was increased to 140°C, final target temperature, in 17 min. The temperatures inside the mixture stabilised after 35 h, and the relative humidity in 1500 h. The equilibrium values of *T* and RH at the end of the heating phase are shown in Figure 14.

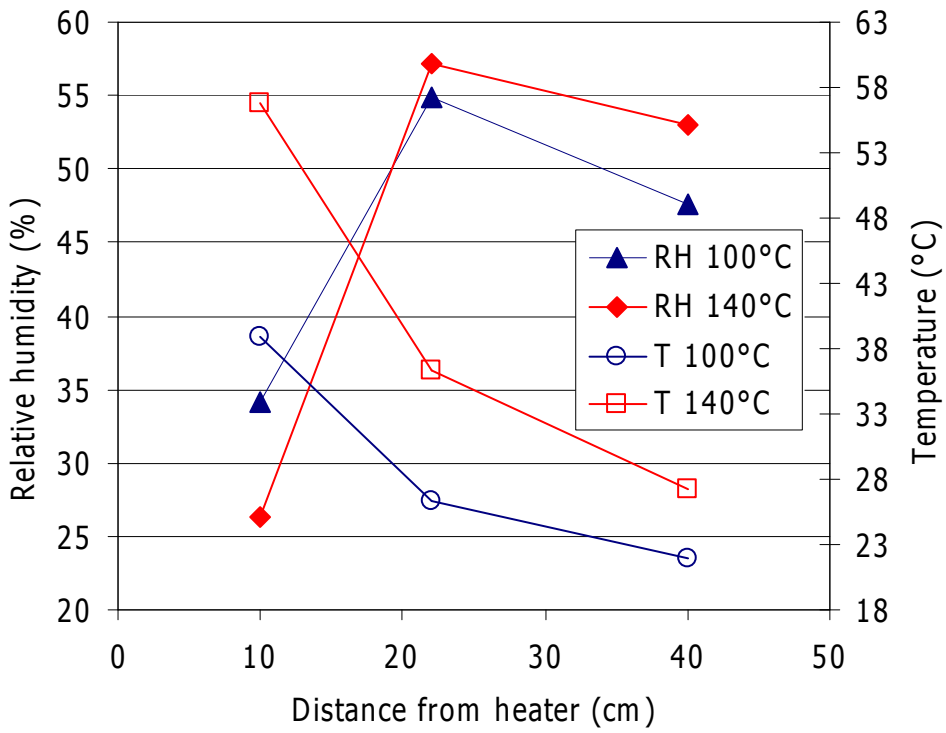

Figure 14: Equilibrium values measured inside the material when the heater was set to 100°C (*t*=3524 h) and 140°C (*t*=5015 h) in cell B

In this cell the axial pressure was also measured on the top of the cell. During the heating phase the pressure was clearly related to temperature, increasing with it. An average value of 0.1 MPa was recorded when the heater temperature was 100°C and of 0.15 MPa when the heater temperature increased to 140°C.

5.2.2 Heating and hydration

After the stabilisation of RH and *T* for heater temperature of 140°C, the hydration line was opened at a pressure equivalent to a 60-cm water column.

Figure 15 shows the evolution of temperature recorded by the sensors from the beginning of hydration (June 2012) to February 2014. The temperatures have kept approximately constant, just reflecting the laboratory temperature oscillation. The average temperature recorded during the hydration phase by sensor 1 (located at 40 cm from the heater) was 25.7±1.8°C, by sensor 2 (at 22 cm from the heater) 35.0±1.6°C and by sensor 3 (at 10 cm from the heater) was 56.5±1.2°C. The temperatures measured on the surface of the cell with thermocouples set on the steel semi-cylindrical pieces are also plotted in the Figure; they also reflect the changes in laboratory temperature. The average temperatures measured at different positions inside and outside the cell (measured with thermocouples as shown in Figure 11) from June 2013 to February 2014 are plotted in Figure 16. The effectiveness of the external isolation is highlighted, as well as the fact that the temperatures inside the bentonite are mostly conditioned by the distance from the heater but not by the distance to the cell axis, which indicates that the temperature distribution followed a uniaxial pattern.

The evolution of relative humidity recorded by the three sensors from the beginning of hydration to February 2014 is shown in Figure 17. The relative humidity kept the same as before hydration for 300 h. Then the sensor located closest to the hydration surface started to record progressively higher relative humidity and stabilised after approximately 540 days at a value of 96%. Sensor 2 recorded a soft decrease in relative humidity down to a value of 50%, and after 130 days it started to record a steady increase. The sensor closest to the heater (sensor 3) was recording a relative humidity of 26% at the beginning of hydration, and this value continue to decrease for 230 days down to 18%; afterwards, there was a very smooth recovery, so that after more than 600 days the initial value was not regained. The overall water intake is also shown in the Figure. The average bentonite water content and degree of saturation after 620 days of hydration, according to the water intake measurement, were 16.1% and 55%, respectively.

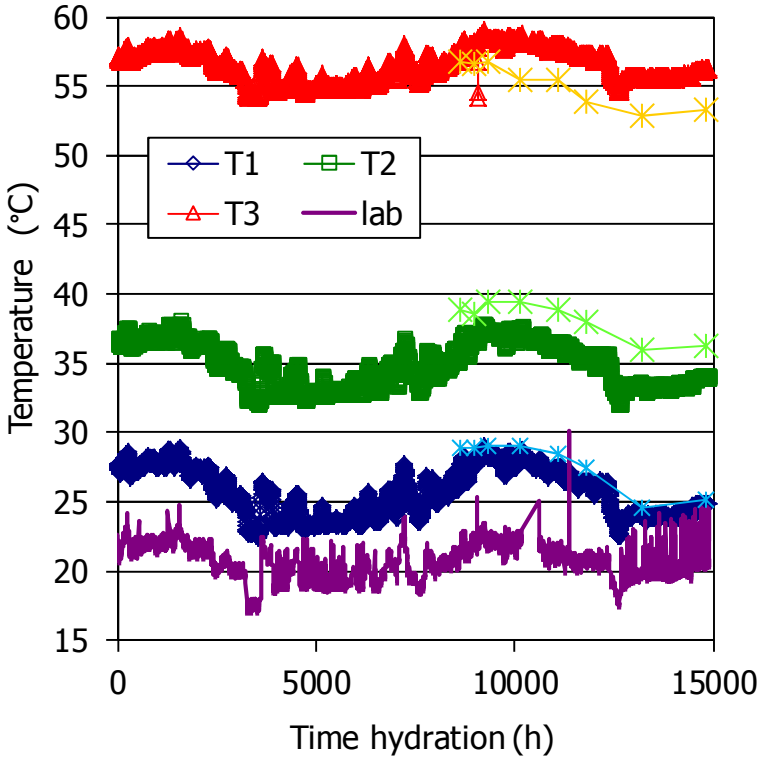

Figure 15: Evolution of temperature in cell B after the beginning of hydration and on the steel surface (crosses) (T1 at 40 cm from the bottom, T2 at 22 cm and T3 at 10 cm)

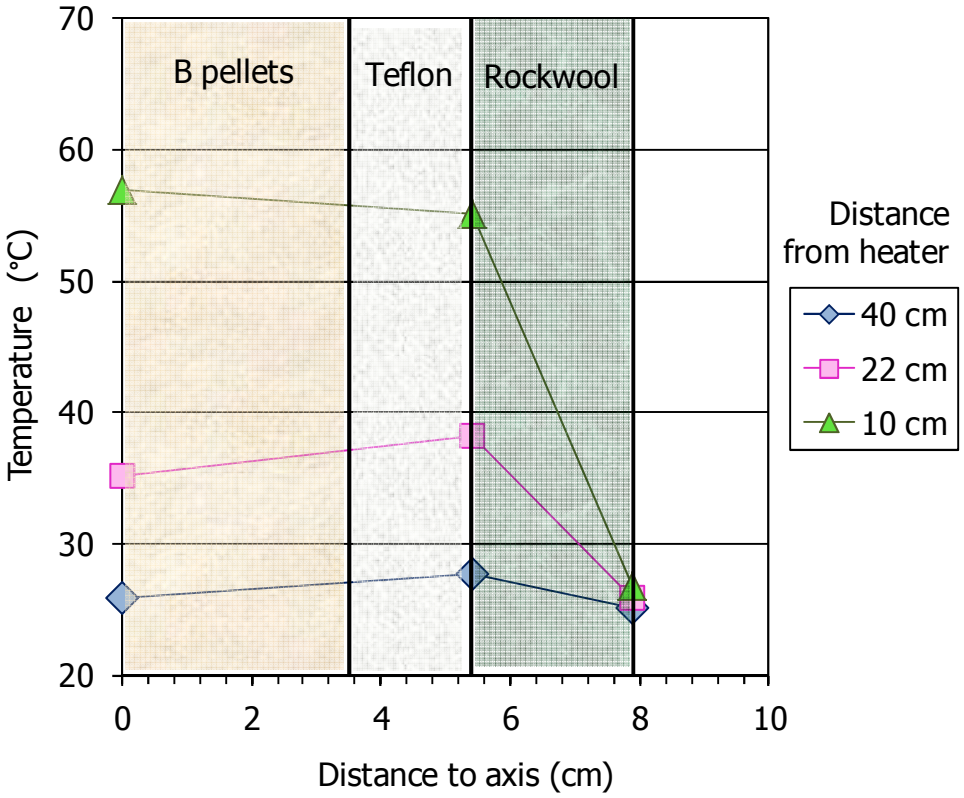

Figure 16: Average temperatures at different distances from the heater in cell B from June 2013 to February 2014 (average laboratory temperature during the period 20.9±1.2°C)

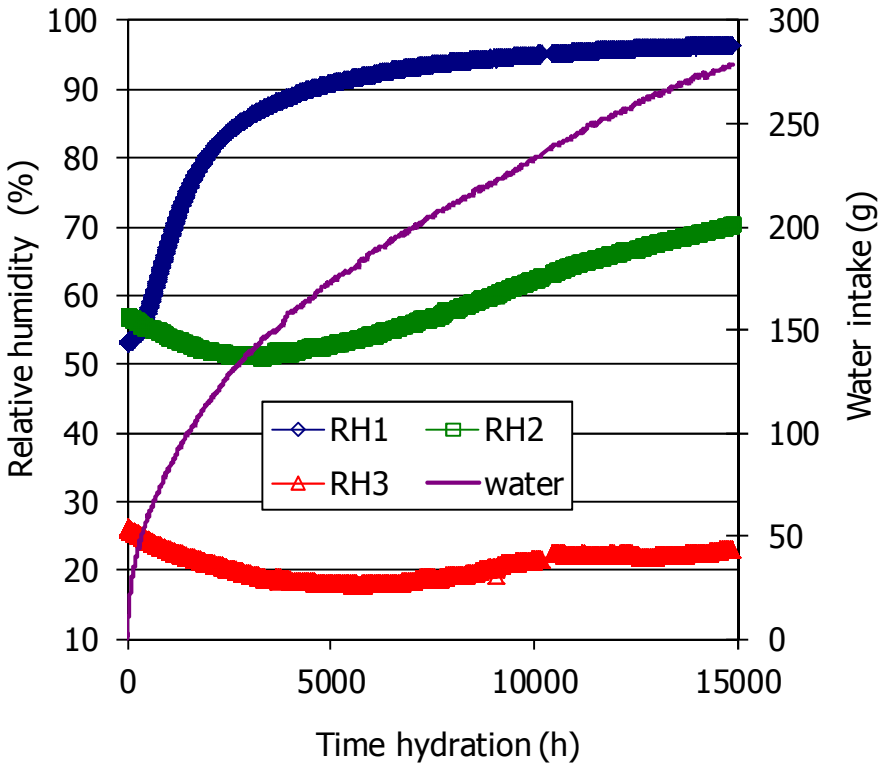

Figure 17: Evolution of water intake and of relative humidity in cell B after the beginning of hydration (sensor 1 placed at 40 cm from the bottom, sensor 2 at 22 cm and sensor 3 at 10 cm)

The heater power was measured during the test, except for the first 1250 h. The improvement of the isolation during the heating phase induced a decrease of the heater power from 12 to 8 W to keep the target temperature of 100°C at the heater surface. When the heater temperature was increased to 140°C, the heater power increased to 12 W and kept around this value (12.0±0.6 W) for the rest of the hydration phase. Nevertheless, there was a slight trend for the power to increase over time during hydration, which would be linked to the increase in thermal conductivity as the bentonite got wetter. Also, the power needed to keep the 140°C on the heater surface was somewhat higher when the external temperatures were lower.

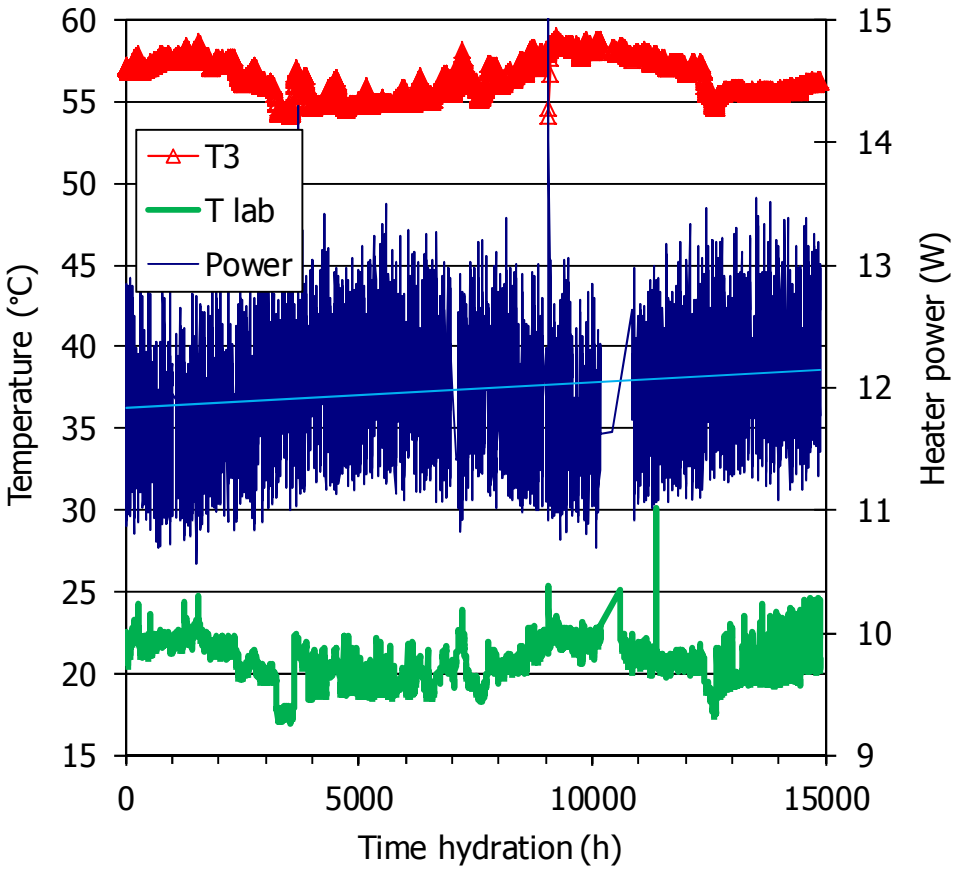

Figure 18: Laboratory temperature, heater power and temperature at 10 cm from the heater (sensor 3) in cell S/B during the hydration phase of the test

The axial pressure measured on top of the cell and the water intake values are shown in Figure 19. Hydration caused a clear increase of the pressure recorded by the load cell located on the top of the cell. This pressure reached a value of 1.4 MPa after 300 days of hydration and kept at approximately the same value still after 620 days of hydration.

A summary of the values recorded during the hydration phase is given in Table A- II in Appendix 1.

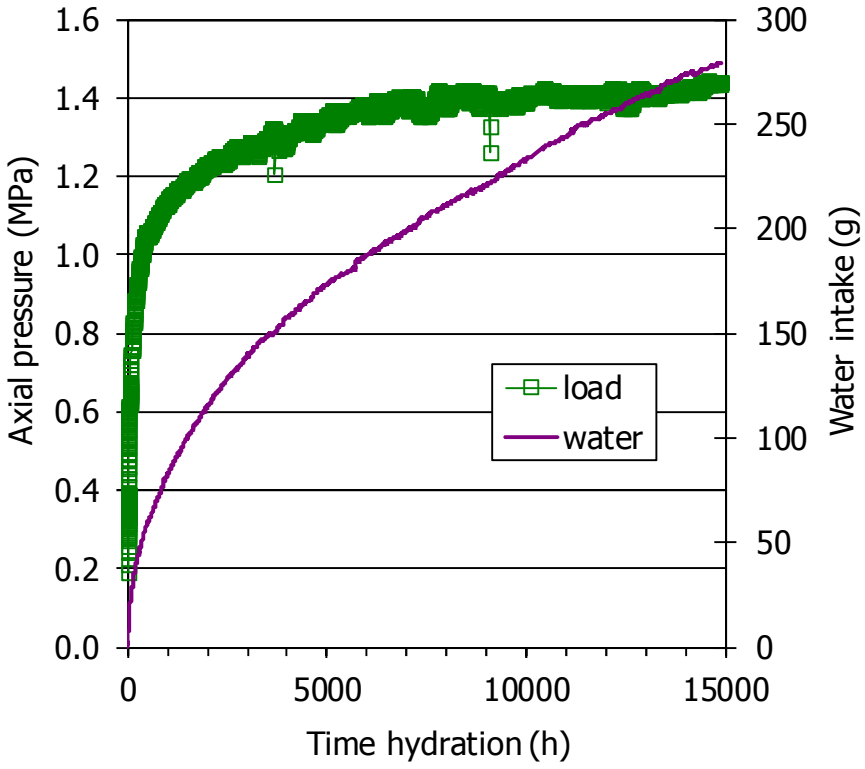

Figure 19: Axial pressure measured on top of cell B and water intake from the beginning of hydration

6 Summary and discussion

The heating phase of both tests showed that the thermal conductivity of the dry materials is low, what caused a high difference in temperature between the heater surface and the sensor located at 10 cm, generating a high thermal gradient near the heater, and low temperatures in the rest of the columns. The stabilisation of the temperature in these materials was very quick, being faster in cell B than in cell S/B. The presence in cell B of the steel reinforcement could be the responsible for the slightly higher temperature measured, despite the fact that the thermal conductivity of the sand/bentonite mixture (before compaction) is higher than that of the bentonite pellets. A reason for this difference could be that the thermal contact between the heater plate and the pellets is better than in the case of the mixture, due to the different granulometry of both materials, which is more heterogeneous for the pellets, allowing for a better filling of pores (Figure 3).

As well, the power needed to keep a given temperature at the heater surface was higher in cell B than in cell S/B (8 *vs*. 7 for heater *T*=100°C and 12 *vs*. 10 for heater *T*=140°C).

The movement of water in the vapour phase as a result of the thermal gradient was evinced by the sharp increase of relative humidity recorded by the sensors closest to the heater –followed by a continuous decrease– and the slower increase recorded by the other two sensors. The different permeability of both materials was made clear in the different pace and extent of this water redistribution process in the vapour phase. Thus, the initial increase of relative humidity at 10 cm from the heater was faster in cell S/B: when the heater was set at 100°C it took 120 h for the RH to reach a peak value of 70% in cell S/B and 300 h to reach a peak value of 57% in cell B. When the heater was set at 140°C it took just 11 h for the RH to reach a peak value at 10 cm from the heater (sensor 3) of 42% in cell S/B and 37 h to reach a peak value of 41% in cell B.

The relative humidity increase in the upper part of the column when the heater was set at 100°C started just after about 20 h in cell S/B and around 1000 h in cell B. Also the relative humidity gradient at the end of the heating phase was sharper in cell S/B than in cell B, due to the lower permeability and higher water retention capacity of the bentonite pellets, which made that before hydration, the higher relative humidity in cell B be recorded in the middle of the column.

The lower permeability of the pellets was again highlighted by the fact that after more than 300 h of hydration, the upper sensor in cell B had not yet recorded any RH change, while by this time the lower sensor in cell S/B had already recorded the arrival of the hydration front.

Figure 20 shows the current temperatures and relative humidities for the two tests (February 2014). Although, as explained above, during the heating phase the temperatures measured were higher in the B cell, this reversed during hydration. The reason is probably the increase in thermal conductivity of the S/B material after being completely saturated. The hydraulic state of both materials is totally different, the S/B mixture having reached full saturation (two of the sensors are flooded) while the B column shows still a steep relative humidity gradient, with approximately the 15 cm closest to the heater having a relative humidity below the initial one.

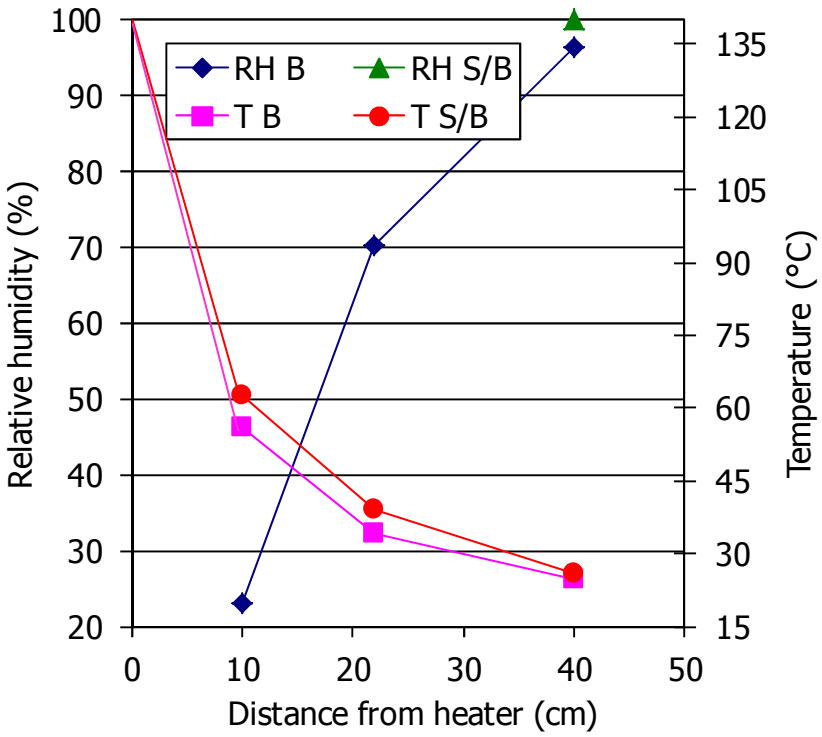

Figure 20: T and RH along the buffer columns after 682 days hydration (cell S/B) and 620 days hydration (cell B)

The axial pressure measured in cell B seems to have stabilised at a value of 1.4 MPa, which is far from the equilibrium swelling pressure value of MX-80 bentonite compacted at dry density 1.53 g/cm^3 (Eq. 1). This is not surprising since the bentonite has still a low degree of water saturation and materials with double porosity (macro/micro) are known to display a non-monotonic development of swelling pressure (Imbert & Villar 2006, Gens et al. 2011). In fact ,in an infiltration test performed with the same material at laboratory temperature (test MGR18, Villar 2013), the swelling pressure measured when the overall water content was the same as that in cell B after 620 days of hydration (16.1%) was 1 MPa, although the final equilibrium axial pressure measured after saturation was 6.5 MPa.

7 References

ENRESA 2005. Ventilation experiment in Opalinus Clay for the management of radioactive waste. Publicación Técnica ENRESA 07/2005. Madrid, 82 pp.

Fernández, A.M. 2011. Determination of the Specific Heat Capacity of materials used as confinement barrier at El Cabril. Interim Report CIEMAT/DMA/2G208/3/11, 26 pp.

Gaus, I., Wieczorek, K., Mayor J.C., Trick T., García-Siñeriz, J.L., Schuster, K., Garitte, B., Kuhlman, U. 2011. EBS behaviour immediately after repository closure in a clay host rock: the HE-E experiment (Mont Terri URL). Proceedings of the 14th Int. Conference on Environmental Remediation and Radioactive Waste Management ICEM'11. September 25-29, 2011, Reims, France. P-59288. ASME, 7 pp.

Gens, A.; Valleján, B.; Sánchez, M.; Imbert, C.; Villar, M.V. & Van Geet, M. 2011. Hydromechanical behaviour of a heterogeneous compacted soil: experimental observations and modelling. Géotechnique 61(5): 367-386.

Imbert, Ch. & Villar, M.V. 2006. Hydro-mechanical response of a bentonite pellets/powder mixture upon infiltration. Applied Clay Science 32: 197-209.

Johnson, L.H., Niemeyer, M., Klubertanz, G., Siegel, P., Gribi, P. (2002): Calculations of the temperature evolution of a repository for spent fuel, vitrified high-level waste and intermediate level waste in Opalinus Clay. Nagra Technical Report NTB 01-04. Nagra, Wettingen, Switzerland.

Pearson F., 1998. Artificial waters for use in laboratory and field experiments with Opalinus Clay *Paul Scherrer Institut. TM 44-98-08*

Plötze M., Weber H.P (2007): ESDRED: Emplacement tests with granular bentonite MX-80: Laboratory results from ETH Zürich. Nagra Arbeitsbericht NAB 07-24. Nagra, Wettingen.

Teodori, S.P., Gaus, I. (Eds.) 2011. Long Term Performance of Engineered Barrier Systems (PEBS). Mont Terri HE-E experiment: as built report. Nagra Arbeitsbericht NAB 11-25. Nagra, Wettingen, 125 pp.

Villar, M.V. 2013. Long-term THM tests reports: Isothermal infiltration tests with materials from the HE-E. PEBS Deliverable 2.2-7.2. CIEMAT Technical Report CIEMAT/DMA/2G210/07/2013. Madrid, 32 pp.

Villar, M.V.; Martín, P.L. & Barcala, J.M. 2005a. Infiltration tests at isothermal conditions and under thermal gradient. Informe Técnico CIEMAT/DMA/M2140/1/05. Madrid, 24 pp. Abril 2005.

Villar, M.V.; Martín, P.L. & Barcala, J.M. 2005b. Modification of physical, mechanical and hydraulic properties of bentonite by thermo-hydraulic gradients. Engineering Geology 81(3): 284-297.

Villar, M.V.; Sánchez, M. & Gens, A. 2008. Behaviour of a bentonite barrier in the laboratory: experimental results up to 8 years and numerical simulation. Physics and Chemistry of the Earth 33: S476-S485.

Villar, M.V.; Martín, P.L.; Gómez-Espina, R.; Romero, F.J. & Barcala, J.M. 2012. THM cells for the HE-E test: setup and first results. PEBS Deliverable 2.2-7.1. Technical Report CIEMAT/DMA/2G210/03/2012. Madrid, 34 pp.

Appendix 1 VALUES RECORDED BY SENSORS

Table A- I: Relative humidity (RH) and temperature (*T*), water intake and laboratory *T* during the hydration phase, which started 3696 h after the beginning of heating in cell S/B (sensor 1 placed at 40 cm from the bottom, sensor 2 at 22 cm and sensor 3 at 10 cm)

Time[a] (h)	Lab *T* (°C)	Heater power (W)	RH1 (%)	T1 (°C)	RH2 (%)	T2 (°C)	RH3 (%)	T3 (°C)	Water intake (g)
0.0	19.8	10.6	82	22.8	77	27.8	24	51.0	37[b]
1.6		9.7	82	22.8	77	27.8	24	51.0	75
2.6		10.0	82	22.9	77	27.9	24	51.1	78
4.6	20.3	10.5	82	23.1	77	28.2	24	51.3	82
10	19.8	10.4	82	23.4	77	28.3	24	51.4	89
24	20.5	9.9	82	23.5	77	28.3	24	51.4	105
51	20.4	9.7	92	23.3	77	28.3	24	51.4	136
99	19.7	9.8	98	23.6	76	28.4	24	51.5	212
123	20.4	9.9	98	23.8	76	28.4	24	51.5	252
147	21.0	9.8	98	24.0	76	28.3	23	51.6	294
171	20.2	10.3	98	24.1	89	27.4	23	51.4	334
275	20.4	9.9	99	24.7	100	31.1	64	45.2	477
315	20.7	10.4	99	24.6	109	32.7	98	48.4	527
459	20.5	11.5	99	26.0	110	37.8	100	60.2	578
603	21.9	12.4	99	28.3	100	40.3	100	63.1	594
747	21.8	11.5	99	28.2	100	40.8		64.7	604
891	21.1	12.5	99	27.4	100	40.3		64.1	607
1063	21.8	13.0	99	28.2	100	42.3		68.0	632
1319	22.3	12.8	99	28.2		41.9		66.7	648
1851	21.6	11.8	99	28.3		41.8		66.6	695
2572	21.9	11.8	99	29.0		42.3		66.7	717
3292	21.5	12.6	99	28.4		41.7		65.9	725
4012	19.7	11.9	99	26.8		40.3		64.7	733
4731	19.1	12.0	99	25.6		39.2		63.7	740
5451	18.5	12.3	99	24.8		38.3		62.7	747
6171	22.0	12.2	99	24.7		38.3		62.6	755
6892	18.7	12.9	98	25.1		38.6		62.8	762
7612	18.9	11.9	98	24.9		38.6		62.7	768

Time[a] (h)	Lab *T* (°C)	Heater power (W)	RH1 (%)	T1 (°C)	RH2 (%)	T2 (°C)	RH3 (%)	T3 (°C)	Water intake (g)
8332	21.1	12.6	98	27.2		40.5		64.2	773
9052	18.8	12.4	98	25.2		38.8		62.8	780
9772	20.7	11.7	98	27.1		40.2		63.9	786
10490	21.8	11.8	100	29.0		41.8		65.0	792
10802	22.7	11.9	99	29.3		41.9		65.0	793
11618	22.8	12.5	101	29.4		41.9		65.0	802
12603	21.3	11.7	99	28.4		41.0		64.0	798
13275	21.2	12.2	100	27.6		40.4		63.6	804
13994	18.5	12.0	99	25.0		38.3		62.0	811
14690	20.2	12.9	99	25.3		38.5		62.2	818
15506	19.5	12.9	99	25.3		38.5		62.2	824
16322	22.9	12.8	100	26.1		39.1		62.8	830

[a]Time since start of hydration; [b]Taken accidentally at the beginning of heating

Table A- II: Relative humidity (RH) and temperature (*T*), water intake, axial pressure and laboratory *T* during the hydration phase, which started 5015 h after the beginning of heating in cell B (sensor 1 placed at 40 cm from the bottom, sensor 2 at 22 cm and sensor 3 at 10 cm)

Time[a] (h)	Lab *T* (°C)	Heater power (W)	RH1 (%)	T1 (°C)	RH2 (%)	T2 (°C)	RH3 (%)	T3 (°C)	Water intake (g)	Axial *P* (MPa)
0.0	22.5	11.3	53	27.5	57	36.6	26.2	57	0	0.19
0.5		12.4	53	27.6	57	36.7	26.1	57	2	0.35
2.5		11.4	53	27.7	57	36.7	26.1	57	4	0.41
4.5	22.1	11.8	53	27.7	57	36.8	26.1	57	6	0.44
12	21.9	11.0	53	27.5	57	36.6	26.1	57	10	0.51
27	21.6	12.1	53	27.6	57	36.7	26.0	57	15	0.59
50	20.5	12.5	53	27.3	57	36.4	25.9	57	20	0.67
75	21.6	11.4	53	27.2	57	36.3	25.8	57	24	0.73
123	21.0	12.2	54	27.4	57	36.6	25.7	57	31	0.82
171	22.3	12.0	54	28.0	57	37.0	25.6	57	35	0.87
219	23.0	12.1	54	28.4	56	37.4	25.5	58	40	0.92
291	21.8	11.2	55	28.0	56	37.2	25.2	58	47	0.97
359	21.1	11.4	56	26.9	56	36.2	24.9	57	51	1.01
363	21.6	11.4	56	27.0	56	36.2	24.9	57	52	1.01
1085	21.9	11.9	69	27.8	54	37.1	22.8	58	85	1.15

Time[a] (h)	Lab *T* (°C)	Heater power (W)	RH1 (%)	T1 (°C)	RH2 (%)	T2 (°C)	RH3 (%)	T3 (°C)	Water intake (g)	Axial *P* (MPa)
1805	21.5	11.1	79	27.1	52	36.4	21.3	57	109	1.20
2525	19.7	11.8	84	25.3	51	34.7	20.1	56	129	1.25
3244	19.1	12.6	87	24.0	51	33.5	19.1	55	144	1.27
3964	18.5	12.9	89	23.2	52	32.7	18.6	55	158	1.28
4684	22.0	11.4	90	23.1	52	32.6	18.2	55	169	1.32
5404	18.7	12.1	91	23.5	54	33.0	18.0	55	178	1.36
6124	18.9	11.6	92	23.3	54	32.8	18.0	55	189	1.37
6844	21.1	11.7	93	25.7	56	34.9	18.4	57	198	1.39
7564	18.8	11.8	94	23.7	57	33.2	18.8	55	207	1.36
8284	20.7	11.7	94	25.8	59	34.9	19.4	57	215	1.40
9002	21.8	12.3	95	28.0	60	37.0	20.4	58	221	1.41
9314	22.7	11.4	95	28.4	61	37.4	21.0	59	225	1.38
10130	22.8	11.5	95	28.5	63	37.6	21.6	59	234	1.41
11116	21.3	11.5	95	27.5	65	36.6	22.3	58	246	1.42
11788	21.2	12.8	96	26.5	66	35.7	22.3	57	252	1.41
12507	18.5	11.6	96	23.7	67	33.1	22.2	55	260	1.38
13203	20.2	12.3	96	24.1	68	33.5	22.1	56	266	1.41
14019	19.5	12.6	96	24.1	69	33.4	22.5	56	274	1.42
14835	22.9	11.6	96	24.9	70	34.1	23.1	56	279	1.44

[a]Time since start of hydration